Potential singularity mechanism for the Euler equations

Michael P. Brenner, Sahand Hormoz, and Alain Pumir

Phys. Rev. Fluids **1**, 084503 — Published 28 December 2016

DOI: 10.1103/PhysRevFluids.1.084503

A potential singularity mechanism for the Euler Equations

Michael P. Brenner,[1] Sahand Hormoz,[2] and Alain Pumir[3]

[1] *School of Engineering and Applied Sciences and Kavli Institute for Bionano Science and Technology, Harvard University, Cambridge, Massachusetts 02138, USA*

[2] *Kavli Institute for Theoretical Physics, University of California, Santa Barbara 93106, USA*

[3] *Univ Lyon, Ecole Normale Supérieure de Lyon, Univ Claude Bernard and CNRS, F-69007, France*

(Dated: December 2, 2016)

Singular solutions to the Euler equations could provide essential insight on the formation of very small scales in highly turbulent flows. Previous attempts to find singular flow structures have proven inconclusive. We reconsider the problem of interacting vortex tubes, for which it has long been observed that the flattening of the vortices inhibits sustained self-amplification of velocity gradients. Here, we consider an iterative mechanism, based on the transformation of vortex filaments into sheets, and their subsequent instability back into filaments. Elementary fluid mechanical arguments are provided to support the formation of singular structure via this iterated mechanism, which we analyze based on a simplified model of filament interactions.

I. INTRODUCTION

The search for singular solutions in the equations of fluid mechanics is tightly related to the formation of small-scales in turbulent flows at high Reynolds numbers. Whereas decades of careful experiments and direct numerical simulations have brought much insight into the statistical properties of the small-scale motion in stationary turbulent flows, surprisingly little is known about the dynamics of energy transfer from large to small spatial scales, either theoretically or experimentally. Qualitatively, the generation of higher harmonics by the nonlinear terms in the Navier-Stokes equations has been recognized by Taylor and Green [1] as a mechanism potentially leading to finite-time infinite gradient.

Establishing the existence of singular solutions of the Navier-Stokes equations is by now regarded as a major open problem in mathematics [2]. Although it has not been possible either to establish or to rule out the existence of singular solutions [3], theorems provide constraints [4–6], and rule out a large class of possible self-similar solutions [7].

The possibility offered by computer technology to simulate flows at high resolution has not led to a clear picture of whether the solutions of the Euler equations blow-up in a finite time [8–13]. So far, numerical work has not revealed any mechanism leading to a self-sustained generation of large velocity gradients in an unbounded fluid. By contrast, convincing numerical evidence for a singular solution to the Euler equation has been found in a fluid with boundary [14]. The observed blow-up, however, crucially rests on unbounded velocity gradients (compression) at the wall. Whether such a singularity can exist in a flow without boundary is far from obvious.

The present paper offers a mechanism that we believe has the potential to both survive as a singular solution of the Euler equation, and even if our construction turns out not to be singular, it offers a way of transferring energy to small scales quickly in a turbulent flow. Our mechanism was inspired by a recent paper of Tao [15], who proposed energy-conserving iterative cascades as a paradigm for singular solutions of Navier Stokes like equations. The construction of [15] is reminiscent of the introduction of shell models, aimed at describing in Fourier space the transfer of energy from large to small scales (energy cascade) in 3-dimensional turbulent flows [16]. Here, we reconsider the problem by looking, in physical space, for an iterative set of instabilities based on known fluid dynamical mechanisms that could potentially lead to a rapid iterative energy cascade. Our construction is based on vortex filament interactions and is depicted in Figure 1. The cascade involves the collision of two vortex filaments, resulting in the formation of two vortex sheets. The sheets then destabilize into filaments, which in turn form new interacting vortex filaments on a smaller spatial scale. The scenario is sufficiently complex that rigorous analysis of whether such a cascade could occur *ad infinitum* is not currently possible. The analysis presented here merely describes the elementary mechanisms that could result in such a cascade. Specifically, we use similarity solutions describing the initial stages of vortex filament collisions, to quantitatively compute how the dimensions of the sheets are related to the initial size and separation of the vortex filaments. We then appeal to classical instabilities of vortex sheets to characterize a mechanism for breakdown of sheets back into filaments. The analysis demonstrates that it is logically possible for an iterative cascade like the one shown in Fig. 1 to exist, and that it would correspond to a finite time singularity of the Euler equation with diverging vorticity. The solution is unstable, and so in practice only a finite number of iterations of the cascade could occur in an experiment.

In what follows, we analyze the vortical interactions leading to this iterative cascade. We begin with two antiparallel vortex filaments separated by a distance R_0 with circulations $\pm\Gamma_0$, and core radius r_0. A scaling analysis based on

similarity solutions shows how the circulation Γ_n, core radius r_n and interfilament separation R_n change at the n^{th} stage of the cascade. We derive a map of the form

$$\Gamma_{n+1} = f(\Gamma_n, r_n/R_n) \tag{1}$$

$$\left(\frac{r}{R}\right)_{n+1} = g(\Gamma_n, r_n/R_n), \tag{2}$$

that predicts how the circulations and vortex configuration evolve from iteration to iteration. Our argument in favor of an iterative cascade rests on plausible approximations that cannot be rigorously proven.

Our attempt to probe various aspects of the mechanisms by using direct numerical simulations runs into the very severe difficulty that the asymptotic regime investigated here is effectively out of reach. In addition to the insight they provide on the interaction of vortex structures, the calculations presented here point to the difficulties in carrying out fully-resolved simulations in the asymptotic regime discussed in this work. A better understanding of the complex processes involved in the interactions of vortex structures is a prerequisite for devising the numerical schemes permitting to simulate blowing-up solutions of the fluid equations.

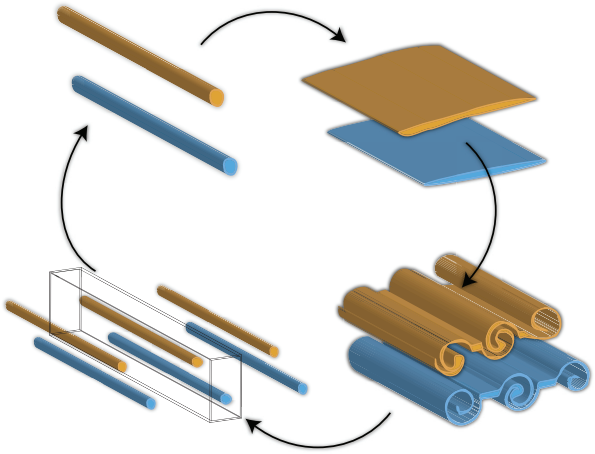

FIG. 1. Schematic of the proposed mechanism for iterated vortex interactions. Initially two antiparallel vortex filaments collide, resulting in the formation of two finite thickness antiparallel vortex sheets. These sheets then destabilize, resulting in two arrays of antiparallel vortex filaments, each of which has a smaller core size, circulation, and separation distance than the initial filaments. The newly formed antiparallel filaments then approach each other and the process continues. This paper carries out scaling estimates based on similarity solutions of the Biot Savart equations and investigates the plausibility of this scenario.

II. INTERACTING VORTEX FILAMENTS

We begin by examining the collapse of interacting vortex filaments as a function of their initial conditions using numerical simulations. When two antiparallel filaments interact [17–20], then either the filaments can directly collide, resulting in a strong deformation of their cores, or they remain at a finite distance to each other without strong core deformation. There is a parameter regime for each behavior depending on the initial shape of the filaments.

To see this, we introduce a continuous family of initial conditions for (the center of the vorticity distributions) of two antiparallel filaments:

$$(x_\pm, y_\pm, z_\pm) = (\pm R_0/2, A_T e^{-z^2/\delta^2}, z) \tag{3}$$

In Eq. (3), the interfilament separation is R_0, A_T is the amplitude of the initial deviation from a straight filament, and δ is related to the minimum radius of curvature ($r_c = \delta^2/A_T$). The vorticity distribution for each filament is gaussian $\omega_\pm(x, y, z_0) \propto \frac{\Gamma_\pm}{r_0^2} \exp(-[(x - x_\pm)^2 + (y - y_\pm)^2]/r_0^2)\ \mathbf{t}_\pm$, where $\mathbf{t}_\pm$ is the direction tangent to the respective curves, and $\Gamma_\pm$ are the enclosed circulations, with r_0 the core size.

Depending on A_T, R_0, δ, the filaments either collide or remain at a finite distance to each other, interacting only weakly. To demonstrate this, we consider two full simulations of the Euler equations, carried out using a standard

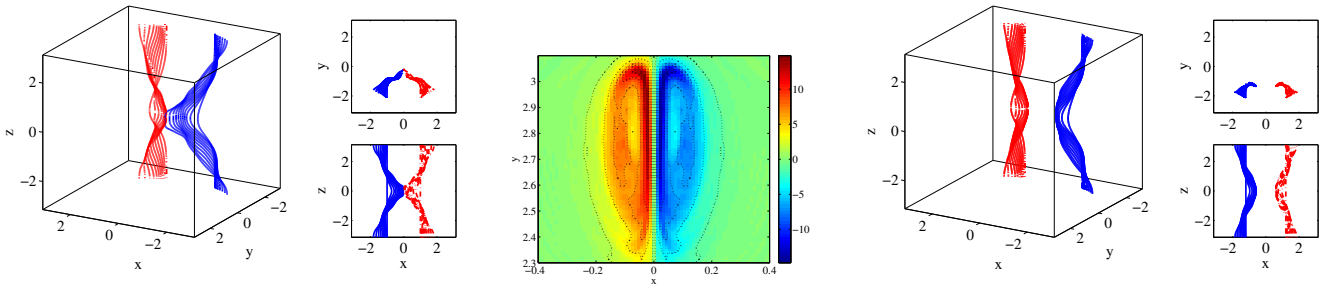

(a) (b) (c)

FIG. 2. Interaction of two filaments with opposite circulation. (a,b): strongly interacting filaments; (c): weakly interacting filaments. The curves in (a) and (c) show the centroid of the vorticity distribution, determined by using the fourth power of the vorticity, at different times, starting from the initial condition until the simulation is terminated. In (a) and (c), the left subpanel shows a particular view of the curves, the upper-right (lower-right) subpanel a view of the filaments from above (from the side). The difference between the two configurations shown in (a) and (c) results from the fact that the filaments in (a) come to contact, contrary to those in (c). The strong interaction, resulting from the contact between the vortices leads to a strong deformation of the vortex cores, leading to the formation of vortex sheets, shown in (b). The parameters of the initial condition are: $R_0 = 2$, $A_T = 1.25$ for (a,b) and $R_0 = 2.4$, $A_T = 1$ for (c).

spectral code [21] in a triply periodic box of size $(2\pi)^3$ at moderate resolutions $(600\times600\times384)$. In the first simulation ($\delta^2 = 1.25$, $r_0 = 0.225$, $A_T = 1.25, R_0 = 2$) (Fig 2a,b), the filaments collide, whereas for the the second example $\delta^2 = 1.25$, $r_0 = 0.225$, $A_T = 1, R_0 = 2.4$) (Fig 2c) they pass through each other, never generating any significant stretching. The direct collision in Fig. 2a causes strong distortion of the core, creating two opposing vortex sheets (Fig. 2b). The sheets become thinner as time goes on, and the simulation had to be stopped when the widths of the vortex sheets are of the order of a couple of grid spacings. The final width is much smaller than the initial vortex core size: $r_0 = 0.225$, by a ratio ≈ 10 (the overall amplification of the vorticity in Fig. 2a is $\lesssim 4$). The deformation of the cores of collapsing vortex filaments causes a significant reduction in the length scale of the vorticity region (at least along one spatial direction), despite only modest amplification of vorticity itself. This reduction in length scales will form a critical component of our iterative cascade.

To conclude this section, we notice that the calculations presented here, as well other comparable numerical simulations, are aimed at providing adequate resolution when the vortex cores of the filaments collapse. The limited number of grid points in all three spatial directions (≈ 1000) prevents to consider a regime where the radius of curvature of the vortex filaments is much larger than the core size. This constraint prevents us from studying directly the regime corresponding to the Biot-Savart approximation, where the radius of curvature remains large compared to all other dimensions [18, 20], and forces us to reconsider the problem of interaction of vortex filaments from a completely different point of view, and to use instead asymptotic considerations.

III. BIOT SAVART SINGULARITIES

The simulations in the previous section show that colliding vortices focus energy from large scales to small scales, with the length scale of the region confining the vorticity decreasing dramatically during the collision. How does the final sheet thickness depend on the initial conditions (A_T, R_0, δ, r_0)? A theory can be constructed starting with a description based on the Biot-Savart law,

$$\mathbf{v}(\mathbf{x}_0) = -\frac{\Gamma}{4\pi}\int \frac{(\mathbf{x}_0 - \mathbf{r}(s))\times\mathbf{t}(s)}{|\mathbf{x}_0 - \mathbf{r}(s)|^3}\, ds, \tag{4}$$

where Γ is the circulation of the filament, $\mathbf{r}(s)$ parameterizes the shape of the filament, with $\mathbf{t}$ is the tangent vector and $\mathbf{x}_0$ is the location where the velocity field is measured. The velocity field at any point in space is the sum of the velocities from all of the different filaments. This approximation accurately captures filament interactions, as long as the core radius of each filament is much smaller than the inter-filament distance. If $\mathbf{x}_0$ is on the axis of a vortex filament, the Biot Savart law (4) is (logarithmically) singular. This singularity is cut off by the finite size of the vortex

core, σ, yielding the regularized Biot Savart law :

$$\mathbf{v}(\mathbf{x}_0) = -\frac{\Gamma}{4\pi}\log\left(\frac{r_c}{\sigma}\right)\kappa\mathbf{b} - \frac{\Gamma}{4\pi}\int_\sigma \frac{(\mathbf{x}_0 - \mathbf{r}(s)) \times \mathbf{t}(s)}{|\mathbf{x}_0 - \mathbf{r}(s)|^3}\, ds. \tag{5}$$

Here $\kappa = r_c^{-1}$ is the curvature of the filament, $\mathbf{b}$ is the binormal vector, and $\int_\sigma$ the regularized integral that runs along the filament. Note that the dynamics of the shape of the vortex filament depends very weakly (logarithmically) on the dynamics of the core (σ); hence the dynamics of the core is decoupled from that of the shape of the filament. In the investigation of the Biot-Savart model in [18, 20], the volume of the core is assumed to be locally conserved. Possible core redistribution along the vortex filament [22], induced by axial pressure gradients, have been shown to be immaterial during the strong interaction studied here [18].

Filament collisions correspond to finite time singularities in the Biot Savart equations. Simulations in both the full Biot Savart equations [18, 20] and a simplified model [23] demonstrate that such singularities exist, with the curvature of the filament diverging as the interfilament separation vanishes. However, the core radius decreases much more slowly than the interfilament separation distance [20], implying that there exists a time before the singularity when the Biot-Savart approximation breaks down, i.e. the core radius is no longer negligible compared with the interfilament separation distance. Therefore, the Biot Savart singularities do not correspond to singularities in the Euler equations. When the assumptions underlying the Biot-Savart approximation break down, another mechanism must take over. Indeed, the full simulations of the direct collision show that the shape of the core distorts significantly and becomes sheet-like. Biot Savart dynamics provide a natural framework for understanding how the characteristic dimensions of this sheet emerges.

A. Similarity Solutions

To proceed further, we need an analytical description of the Biot Savart singularity, in the regime before the core radius is of order the interfilament separation distance. The first step is to construct a similarity solution to the governing Biot Savart equations [20]. From dimensional analysis, the characteristic length scale governing filament shape is $\ell(t) = \sqrt{\Gamma(t^* - t)}$, where Γ is the magnitude of the circulation, and t^* the time of singularity. The shapes of the filament $\mathbf{r}_i(s,t)$ then take the form

$$\mathbf{r}_i(s,t) = \ell(t)\mathbf{G}_i(\eta), \tag{6}$$

where $\eta = s/\ell(t)$, and s measures arc length along the filament. Plugging this ansatz into Eq. 5 gives a set of coupled ordinary integro-differential equations for the shapes of the filament. These equations can be solved by reducing them to a set of delayed differential equations[20]. The similarity solution corresponds to a double tent like structure, see Fig. 3, in which the filaments collide in finite time.

Critically, the details of the collapsing geometry, such as the angles between the arms of the tent, depend on the initial conditions [20]. When mapping $\mathbf{G}$ back to real space using Eq.(6), the geometry in similarity space determines the prefactors of the scaling laws associated with the collapse in real space. For example, the separation distance between the filaments in similarity space, D, becomes the prefactor of the scaling law for the inter-filament separation distance, $D\sqrt{\Gamma(t^* - t)}$. We will see below that these prefactors critically determine the properties of the iterative cascade. The existence of potentially singular cascade relies on finding collapse geometries that lead to desired ranges for the prefactors.

Analysis of the similarity solutions demonstrates [20] that the core radius *always* decreases more slowly than the interfilament separation distance, so that the Biot Savart dynamics necessarily break down before the singularity, consistent with what is seen in simulations. However, a striking and corresponding feature of the similarity solution is that when the filaments collide, they remain nearly parallel for all times, even when the filament curvature diverges. We will exploit this feature to understand the deformation of the filament cores using the similarity solution.

IV. FROM FILAMENTS TO SHEETS

We turn to a quantitative description of how the filaments transition to sheets. In this section, the vortex filaments/sheets are assumed to be well-separated, so the Biot-Savart description applies. Appendix A, which rests on a multipole expansion of the vorticity field, shows that provided the separation between the filaments is large compared to the spatial extent of the cores, the Biot-Savart description used in [20] is justified. As a singularity develops, each filament produces a large strain $\nabla\mathbf{v}$ at the other filament, which can be broken down into a component along the direction of the filament $\partial_{||}v = (\mathbf{t}\cdot\nabla)\mathbf{v}\cdot$ as well as components that are perpendicular $\nabla_\perp\mathbf{v}$. The strain along

the filament $\partial_{||} v$ causes stretching – which as already mentioned does not happen quickly enough for the filament approximation to be uniformly valid. This means that $\nabla_\perp \mathbf{v}$ stretches out the (initially circular) filament shape into a different shape.

How these velocity gradients change the shape of the filament can be computed directly, since the filament remains nearly parallel as the singularity is approached. This means we can approximate the cross section as a two dimensional slice, with out of plane stretching. Building on work of Kida [24], Neu [25, 26] showed how to compute the dynamics of an initially circular patch of vorticity in the plane subject to both in plane shear, and out of plane stretching. The approach developed in these works assumes a uniform distribution of vorticity inside the patches. This is a simplifying assumption when describing interacting vortex structures in a genuine 3-dimensional flow, which does not affect the conclusions of the analysis presented here. Given a velocity field of the form

$$\mathbf{u_s} = \gamma' x\hat{x} - \gamma y\hat{y} + \gamma'' z\hat{z}, \tag{7}$$

with incompressibility implying $\gamma' - \gamma + \gamma'' = 0$, if $a(t), b(t)$ are then the lengths of the major and minor axis of an ellipse, corresponding to the shape of the deformed filament core, and $\theta(t)$ is the angle that the major axis makes with the $\hat{x}$ axis, then[26]

$$\dot{a} + \Big(\gamma \sin^2(\theta) - \gamma' \cos^2(\theta)\Big) a = 0 \tag{8}$$

$$\dot{b} + \Big(\gamma \cos^2(\theta) - \gamma' \sin^2(\theta)\Big) b = 0 \tag{9}$$

$$\dot{\theta} = \frac{\Gamma}{(a+b)^2} - \frac{1}{2}(\gamma + \gamma')\frac{(a^2+b^2)}{a^2-b^2}\sin^2(\theta). \tag{10}$$

The change in filament shape can be computed by applying these equations to the similarity solution, using Eqn. 6, together with the Biot Savart law for the velocity field Eq. 4 to compute $\nabla \mathbf{v}$ that one filament produces at the location of the other. Eqns. (8,9,10) then give the time dynamics of the shape of the center line.

At the level of scaling, we can anticipate the form of the solution: Given that $\ell = \sqrt{\Gamma(t^* - t)}$, the Biot Savart equation implies $\nabla \mathbf{v} \sim \frac{\Gamma}{\ell^2} = (t^* - t)^{-1}$. Hence, $\gamma = \alpha(t^* - t)^{-1}$ and $\gamma' = \beta(t^* - t)^{-1}$for some coefficients α, β. The prefactors depend on the location along the similarity solution, since different positions along the filament experience different shears. Anticipating that $a \sim (t^* - t)^{-A}$ and $b \sim (t^* - t)^B$, with $A, B > 0$ (since the major axis will diverge while the minor one will vanish as the singularity approaches), it can easily be seen that Eqn. 10 implies $\theta \to 0$, so the major axis of the elliptical cross section aligns with the principal straining direction of the flow. This then simplifies the equations for a, b to

$$\dot{a} - \gamma' a = 0 \tag{11}$$

$$\dot{b} + \gamma b = 0, \tag{12}$$

implying that $A = \beta$ and $B = \alpha$. These are the laws for the flattening of the core of the vortices into filaments. Strikingly, the scaling exponents for the stretching of the vortex filaments are determined by the *prefactors* of the Biot Savart similarity solution.

Now, we can use these laws to predict filaments deformation. Suppose that our two vortex filaments start out a distance R_0 apart, with an initial radius of r_0, and assume the interfilament distance is much larger than the filament radius, $R_0 \gg r_0$. The inter filament separation decreases as $R(t) = \sqrt{\Gamma(t^* - t)}$, so that the initial separation is $R_0 = \sqrt{\Gamma t^*}$. This gives the dependence of the singular time on the initial interfilament separation.

This core stretching implied by the Biot-Savart singularity stops when the interfilament separation equals the major axis length of the cross section, as justified in Appendix A. At this point the strong shear causing the filament to stretch into a sheet will stop. This condition is

$$R(t) = a(t) \quad \sqrt{\Gamma(t^* - t)} = r_0 \left(\frac{t^*}{t^* - t}\right)^\beta, \tag{13}$$

which gives the time at which the stretching stops. At this time, the distance between the filaments is

$$\frac{R_{\text{def}}}{R_0} = \left(\frac{r_0}{R_0}\right)^{1/(1+2\beta)}. \tag{14}$$

This allows us to compute both a and b when the stretching is over. Since $a = R_{\text{def}}$, we have

$$a = r_0 \left(\frac{R_0}{r_0}\right)^{2\beta/(1+2\beta)} \quad \text{and} \quad b = r_0 \left(\frac{R_0}{r_0}\right)^{-2\alpha/(1+2\beta)}. \tag{15}$$

Thus at every stage, both a and b are set by the ratio of the initial filament separation to the initial core radius. These laws are entirely geometric, and independent of Γ, which only sets the time scale.

V. FROM SHEETS TO FILAMENTS

Given the scales of the sheets that form from the collision of two filaments, we now turn to study how these sheets destabilize into filaments. Standard hydrodynamic instability results suggest an obvious mechanism, namely the Kelvin-Helmholtz instability. A vortex sheet is intrinsically unstable to perturbations of wavelengths larger than the width of the sheets. In his pioneering article, Rayleigh [27] established that the most unstable mode has a wavelength ≈ 8 times the width of the layer. The precise value of the most unstable wavelength depends on the detail of the structure of the sheet ; in his original calculation [27] assumes a piecewise velocity distribution. In the following, we merely assume a linear relation between the most unstable wavelength λ and the width of the vortex sheet, b:

$$\lambda = Cb \tag{16}$$

where C is some constant.

Whether it is appropriate to use the estimate based on Rayleigh theory ultimately rests on the relative importance of the stretching terms, introduced in Eq. (7) and the growth rate of the instability in the absence of any stretching can in principle be done by using the asymptotic approach developed in [28]. Generically, the stretching terms are $\gamma \approx \Gamma/\ell^2$, where ℓ is the distance between the structures. On the other hand, the velocity difference across a vortex sheet is of the order of Γ/a, so the growth rate of the instability is $\sigma \approx 2\pi\Gamma/(ab)$. In these terms, provided $\ell \gg \sqrt{4ab/\pi}$, the stretching terms in Eq. (7) is a minor perturbation to the main mechanism of instability. It is a simple matter to check that, under the conditions of the iterations presented in Section VI, these conditions are satisfied, which justifies the use of Eq. (16). We will typically take the original value $C \approx 8$ for explicit calculations, although the precise value will turn out to be immaterial for our purpose, provided $C > \pi$, as discussed below– see, e.g. Eqn. (22).

The initial vortex sheets have width b, length a, and let Γ be the total circulation in the sheet. Once the instability has developed, the vortex sheet breaks up in $\approx (a/\lambda)$ pieces, each carrying a fraction (λ/a) of the original circulation:

$$\Gamma_{new} \approx \frac{\lambda}{a}\Gamma = C\frac{b}{a}\Gamma \tag{17}$$

It is worth remarking that this classical Rayleigh mechanism is not the only possible way for transforming sheets to filaments; this is just the simplest possibility. In Appendix B, we show numerical results that suggest a different mechanism for concentrating vorticity from sheets to filaments. There are presumably other possibilities as well.

VI. ITERATING THE INSTABILITY

Thus far, we have demonstrated that two vortex filaments with circulations $\pm\Gamma$ come together to form two vortex sheets, with elongations depending on the initial separation of the filaments and their initial radius. The sheets then destabilize into new filaments, with a new circulation. Note that the sign of the circulation of the vortex filaments is conserved throughout this process, i.e. positive circulation vortex filaments make positive circulation vortex filaments, and vice versa.

We now consider whether this construction can iterate *ad infinitum*. Let us denote r_n the radius of the vortex filament at the n^{th} stage of the iteration, and R_n the separation at this stage. Let Γ_n be the circulation, and a_n, b_n be the dimensions of the sheet at the n^{th} iteration. We assume in what follows that the α and β are constant, and moreover that the geometries are such that the instability can really iterate. We remark that this is probably the most suspect step in our derivation, and certainly the most difficult to prove theoretically. It is necessary to know the geometry of the filaments from iteration to iteration of the cascade, and to determine whether there exist conditions for them to iteratively interact. Here we assume that such iterative interaction is possible and examine the scaling consequences of it.

From Eqn. (15) we have

$$\frac{a_n}{b_n} = \left(\frac{R_n}{r_n}\right)^{\frac{2(\beta+\alpha)}{(1+2\beta)}}, \tag{18}$$

The sheets undergo the Kelvin-Helmholtz instability, resulting in domains with size λ, Eqn. (16), and thickness b_n. The circulation at the next iteration is therefore

$$\Gamma_{n+1} = C\Gamma_n\left(\frac{b_n}{a_n}\right) \tag{19}$$

After the sheet undergoes instability, new patches of vorticity form, with an area approximately $b_n\lambda \approx Cb_n^2$. This area forms the cross section of the next iteration of tubes. Assuming a circular cross section, the new tube radius must satisfy,

$$r_{n+1} = \sqrt{\frac{C}{\pi}} b_n \tag{20}$$

We can use Eq.(18) to solve for b_n and plug into the above equation. Then since the distance between the two vortex filaments at stage $n+1$ is equal to $R_{n+1} = a_n$, the ratio r_{n+1}/R_{n+1} must obey

$$\frac{r_{n+1}}{R_{n+1}} = \sqrt{\frac{C}{\pi}} \Big(\frac{r_n}{R_n}\Big)^{\frac{2(\alpha+\beta)}{1+2\beta}} \tag{21}$$

A. Iteration map

Equation (21) defines a simple map, which can be best studied by introducing the variable: $x_n = \ln(\frac{r_n}{R_n})$, implying

$$x_{n+1} = \frac{1}{2}\ln(\frac{C}{\pi}) + \frac{2(\alpha+\beta)}{1+2\beta}\ x_n \tag{22}$$

The iteration has a fixed point, x_∞, given by

$$x_\infty = \frac{(1+2\beta)}{2(1-2\alpha)}\ln(\frac{C}{\pi}) \tag{23}$$

Since $\pi < C \approx 8$, the fixed point $x_\infty < 0$ so that $(r_n/R_n) < 1$, provided $\alpha > 1/2$. The iteration is stable if $\frac{2(\alpha+\beta)}{1+2\beta} < 1$, which is satisfied only if $\alpha < 1/2$. Since fixed points only occur when $\alpha > 1/2$, this implies all fixed points are unstable.

B. Vanishing length scales and time scales of the solution

Next, we derive explicit expressions on how the temporal and spatial scales of the solution diminish at each iteration of the cascade. To do so, we first write down an equation relating the spatial length scale r_{n+1} to r_n. Plugging the expression for b from Eq.(15) into Eq.(20) gives,

$$r_{n+1} = \sqrt{\frac{C}{\pi}}(\frac{r_n}{R_n})^{2\alpha/(1+2\beta)} r_n \tag{24}$$

At the fixed point of the cascade, the ratio r_n/R_n is a constant $r_n/R_n = (C/\pi)^{\frac{(1+2\beta)}{2(1-2\alpha)}}$, which implies $r_{n+1} = \mu_X r_n$, where $\mu_X \equiv (C/\pi)^{\frac{1}{2(1-2\alpha)}}$ is the factor by which the length scale shrinks at every iteration. Similarly, the time scale, given by R_n^2/Γ_n, is multiplied between step n and $n+1$ of the iteration, by $\mu_T \equiv \frac{1}{\pi}(\frac{C}{\pi})^{\frac{\alpha-\beta}{1-2\alpha}}$.

When $\alpha > 1/2$ and $\alpha > \beta$, both $\mu_X < 1$ and $\mu_T < 1$, implying that spatial and temporal scales shrink from one step of the cascade to the next. If we assume that the dynamics repeats itself from one iteration to the next, the condition $\mu_T < 1$ ensures that the time from the first step of the cascade up to $n \to \infty$ is bounded by the geometric sum:

$$T_{sing} = T_0 \sum_{n=1}^{\infty} \mu_T^n = T_0 \frac{\mu_T}{1-\mu_T} < \infty \tag{25}$$

which is sufficient to ensure that infinitely small scales are formed in a finite time.

To check for self-consistency, we estimate the amplification vorticity as a function of the time to the occurrence of singularity, T_{sing}. The time to singularity at the n^{th} iteration of the cascade is $T_{sing} - T_n$. n^{th} iteration of the cascade happens at time $T_n = T_0\mu_T\frac{(1-\mu_T^{n+1})}{(1-\mu_T)}$, therefore, $T_{sing} - T_n = T_0\frac{\mu_T^{n+2}}{(1-\mu_T)} \propto \mu_T^n$. Clearly, at each iteration, the vorticity is amplified by μ_T^{-n}. Together, these estimates imply that the vorticity grows, as time gets closer to the singular time,

as $|\omega| \propto 1/(T_{sing} - T)$. This scaling laws is consistent with the exact result [5], which states that for a singularity to occur, the extremum of vorticity must grow at least as fast as $1/(T_{sing} - T)$,

In contrast, the velocity field is amplified by $(\mu_x/\mu_T)^n$ by the n^{th} iteration of the cascade, where μ_X^n is the cumulative reduction in the spatial scales since the first iteration. Expressing the velocity amplification in terms of the time to singularity gives $1/(T_{sing} - T)^p$, with $p = 1 - \ln(\mu_X)/\ln(\mu_T)$. Unlike vorticity, the velocity field amplifies with an exponent which depends on the details of the solution.

Lastly, we check some of the assumptions used to estimate how the length and time scales vanish at each iteration of the cascade. In using the estimate that the time necessary from one step of the cascade to the next scales like R_n^2/Γ_n, we have assumed that the dynamical process leading to step n to $n+1$ proceeds in a self-similar fashion, with exactly the same process occurring at each iteration, and thus involves only the available scales at step n. At the level of scaling, this notion is not inconsistent: If, at the n^{th} stage, we start from two antiparallel filaments of core size r_n, separated by a distance R_n, then the separation between the two filaments obeys $R(t) \approx D\sqrt{\Gamma_n(t_* - t)}$, with $R_n = D\sqrt{\Gamma t_*}$. Here D is a constant assumed independent of n. Thus, the time for the filaments to get to a distance a_n is $a_n^2/(D^2\Gamma_n) = 1/D^2\ R_n^2/\Gamma_n\ (r_n/R_n)^{\frac{2}{1+2\beta}}$. Correspondingly, the time for a Kelvin-Helmholtz instability for a vortex sheet of width b_n and with a velocity jump of order $\approx \Gamma_n/a_n$ to develop is of the order $(a_n b_n)/\Gamma_n$. The instability thus develops faster than the time needed to bring the filaments together, by a factor $\sim (b_n/a_n) \ll 1$. Together, these results motivate that the dominant contribution to the time scale of each iteration of the cascade is given by R_n^2/Γ_n.

C. Estimating prefactors from the Biot-Savart solutions

Finally, we discuss the possible values for α and β, the prefactors of the scaling law of the straining velocity field, to determine whether there exist solutions that satisfy $\alpha > 1/2$ and $\alpha > \beta$ for a potentially singular cascade. The prefactors can be derived from the Biot-Savart similarity solutions by directly computing the strain field. The velocity field acting on point s of one filament induced by the other filament follows from plugging the similarity solution (Eq.(6)) into the Biot Savart equation:

$$\mathbf{v}(s) = \frac{\sqrt{\Gamma}}{2\pi\sqrt{t^* - t}} \frac{(\mathbf{G}_1(\eta) - \mathbf{G}_2(\eta_2)) \times \mathbf{G}_2'(\eta_2)}{|\mathbf{G}_1(\eta) - \mathbf{G}_2(\eta_2)|^2}, \tag{26}$$

where $\eta = s/l(t)$ and η_2 is the point on filament 2 closest to point η on filament 1. In this equation, we have approximated the shape of the filaments in similarity space $\mathbf{G}_{1,2}(\eta)$ as straight lines [20] (note that when mapped back to real space the curvature at the point of approach still diverges). The strain tensor follows from Eq.(26),

$$\frac{\partial \mathbf{v}}{\partial x} = \frac{1}{2\pi(t^* - t)} \frac{\partial}{\partial \bar{x}} \left[\frac{(\mathbf{G}_1(\eta) - \mathbf{G}_2(\eta_2)) \times \mathbf{G}_2'(\eta_2)}{|\mathbf{G}_1(\eta) - \mathbf{G}_2(\eta_2)|^2} \right], \tag{27}$$

where $\bar{x} = x/l(t)$ denotes the scaled coordinates in similarity space. Assume that the tangential vector of the filaments is along the $\hat{z}$ direction such that the velocity field only varies along the $\hat{x}$ and $\hat{y}$. The two-dimensional strain is given by,

$$\begin{pmatrix} \delta v_x \\ \delta v_y \end{pmatrix} = \frac{1}{2\pi(t^* - t)} \begin{pmatrix} 0 & 1/D^2 \\ 1/D^2 & 0 \end{pmatrix} \begin{pmatrix} \delta x \\ \delta y \end{pmatrix} \tag{28}$$

$D = |\mathbf{G}_1(\eta) - \mathbf{G}_2(\eta_2)|$ is the separation distance between the two filaments in similarity space and sets the scaling law $R(t) = D\sqrt{\Gamma(t^* - t)}$. It is easy to show that a $\pi/4$ rotation of the coordinate axes, maps the Taylor expansion of the velocity field in Eq.(28) to exactly the velocity field assumed in Eq.(7). It follows that

$$\alpha = \frac{1}{2\pi D^2} \tag{29}$$

The straight filament approximation implies that $\alpha = \beta$, which follows from the divergence free condition of the velocity field in the two reduced dimensions. To check that $\alpha > \beta$, we must consider velocity along the filament axis, $\hat{z}$. Assume that the filament has a small but non-zero curvature at point s, resulting in $v_z \neq 0$. If there is vorticity amplification at point s the filament must stretch at that point, or equivalently $\frac{d\mathbf{v}}{ds} \cdot \mathbf{t} > 0$. Since the tangential vector $\mathbf{t} \approx \hat{z}$, it follows that $\gamma'' > 0$ in Eq.(7). To satisfy the incompressibility condition $\gamma' - \gamma + \gamma'' = 0$, we must have that $\alpha > \beta$.

Finally, we note that Eq.(29) implies that $\alpha > 1/2$ for at least some initial conditions. Because the self-similar collapse geometry, $\mathbf{G}$, is not universal, it permits a range of possible values of D. These different collapse geometries

presumably depend on the initial conditions of the vortex filaments. Fig.3 shows two examples of such geometries computed using the framework presented in [20]. Moreover, numerical simulations of collapsing vortex filaments in [29] arrived at $D \approx 0.47$, for which $\alpha > 1/2$. Recent work in [30] also provides an approximate analytical expression for D as a function of the collapse geometry, which also permits values of D that result in $\alpha > 1/2$.

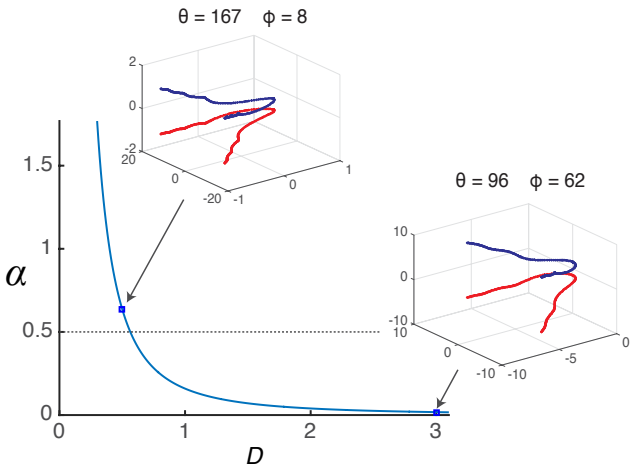

FIG. 3. Relationship between α, the pre-factor of the scaling law of the velocity field in the $\hat{y}$ direction and D the pre-factor of the scaling law of separation distance between a pair of collapsing vortex filaments. The insets show possible geometries of the collapse, or the similarity solution $\mathbf{G}$, at two different values of D. θ is the opening angle of the two arms of the same filament, and ϕ is the angle between one arm of the top filament and the corresponding arm on the bottom filament. For a cascade that is potentially singular, we must have $\alpha > 1/2$. For details of how the similarity solutions are calculated see [20].

As already stressed, our approach may possibly leave aside some important physical effects, which could modify significantly the solution, even at a qualitative level. This includes the effect induced by an axial pressure gradient, resulting from the inhomogeneity of the core radius, which tends to oppose stretching [22]. The estimates of [18] indicate that the core redistributions induced by this mechanism are slow, during the fast collapse process considered here [18, 20]. Although, for reasons already explained (see Section II), our simulations are not in the proper asymptotic regime, they allow us to directly determine the evolution of a and b from direct numerical simulations of the Euler equations. We observe a fast decay of b and a slower increase of a, which can be plausibly represented by power laws, $b(t) \propto (t^* - t)^{\alpha}$ and $a(t) \propto (t^* - t)^{-\beta}$, which values of $\alpha \approx 1$ and $\beta \approx 1/3$, see Appendix C.

VII. CONCLUSION

This article was motivated by the recent suggestion by Tao [15] that the solutions of the Navier-Stokes/Euler equations may become singular, by transferring energy from larger scales to smaller scales, through a non-trivial dynamical process, where the mechanism of transfer repeats itself *ad-infinitum*. This process is globally self-similar, in the sense that transferring energy from one scale to the next is independent of the absolute scale. This scenario is very reminiscent of the numerical observations in [18, 31], see also [32].

Whereas the explicit model in [15] does not obviously relate to any fluid mechanical process, our construction here rests exclusively on well-known fluid mechanical mechanisms. Namely, we started from solutions of the Biot-Savart model consisting of two antiparallel vortex filaments, with negligible core diameters, which collapse towards each other and potentially generate infinite stretching in a finite time. However, eventually, the separation distance between the filaments becomes smaller than the core diameters, making the Biot-Savart approximation inconsistent. As the Biot-Savart approximation breaks down, the filaments are stretched and form vortex sheets, which in turn are subject to the well-known Kelvin Helmholtz instability. This leads subsequently to the formation of a new set of antiparallel vortex filaments. Under a set of consistent approximations, we found that this process can repeat itself, as sketched in Fig. 1, generating an infinite velocity gradient in a finite time. Estimates, based on known asymptotic results, allow us to provide a semi-quantitative description of the process.

The mechanism proposed here rests on approximations which are consistent from a fluid mechanical point of view. Although plausible, our central assumption, that the filaments created from one iteration of the process lie in the basin

of attraction for a new Biot Savart singularity, is more difficult to prove. Available numerical work, including the work carried out here with limited numerical resolution, has not allowed us to reach the asymptotic regime described here. In fact, consistent with previous numerical work, we observe formation of vortex sheets which get squashed towards each other, which in practice corresponds to a narrow jet. Although this flow configuration is unstable, potentially leading to a vortex roll-up and in turn to formation of vortex tubes, we did not observe any trace of the jet instability. The roll-up mechanism, potentially leading to the formation of vortex tubes from the parallel sheets, comes from a mechanism which can be qualitatively understood. Whether it is possible to construct an iterative solution based on this roll-up process remains to be seen; answering this question requires a more quantitative analysis, beyond the classical instability results [27]. In general, the transition from sheets to filaments may involve mechanisms which differ from those investigated here.

We conclude by stressing that the ideas developed in this work are of much broader impact than just the singularity problem studied here. The notion that complex fluid mechanical phenomena may be understandable in terms of *unstable* limit cycles is already familiar in other contexts related to turbulence, in particular in pipe flows at high Reynolds numbers. The work done in this context [33] provides a general framework to explore the influence of the unstable solutions on the flow. The difficulties already mentioned to carry out numerical simulations in the appropriate asymptotic regime, however, are likely to significantly hinder the extension of the approach used in pipe flows to the singularity problem.

The specific question of interaction between vortex filaments in an inviscid fluid is deeply related to the problem of vortex reconnection in the presence of viscosity [9, 34]. At low Reynolds numbers, reconnection occurs in a seemingly simple (laminar) way [35–39]. The process can be described by an elegant model [40], which very successfully reproduces the main features obtserved in low-resolution numerical studies [41]. On the other hand, at higher Reynolds numbers, experimental evidence points to the formation of instabilities during the reconnection process, thus leading to a much more complex process than described in [40]. The generation of increasingly complex structures is at the heart of the mechanism proposed here.

Finally, despite nearly a century of study, remarkably little is understood about the temporal progression of energy from large scales to small scales in turbulent flows. Although the relation between solutions of the Euler equations studied here and the mechanisms involved in turbulence is not obvious, the possibility that the Kolmogorov turbulent energy cascade may involve iterations is intriguing, and worth further investigations.

Acknowledgements: We are greatly indebted to Leo Kadanoff for past support and encouragement, and in particular, for sparking MPB's interest in this problem as a graduate student by giving him a paper of AP [42] to read. This research was funded by the National Science Foundation through the Harvard Materials Research Science and Engineering Center DMR1420570 and the Division of Mathematical Sciences DMS- 1411694. MPB is an investigator of the Simons Foundation.

APPENDIX A: CORRECTIONS TO THE BIOT-SAVART MODEL: MULTIPOLE EXPANSION

The goal of this appendix is to carry out a multipole expansion of the Biot-Savart law. We want to demonstrate that the formalism that we are using for the Biot-Savart singularities also applies when the distribution of vorticity inside the sheet is arbitrary – one does need to assume any particular distribution of vorticity. The only condition that applies is that the extent of the vorticity distribution is smaller than the interfilament separation.

To begin, we start with some vector identities. Given that the vorticity $\omega = \nabla \times \mathbf{v}$, we have that

$$\mathbf{v} = -\frac{1}{4\pi}\int \omega \times \nabla \frac{1}{|\mathbf{x}-\mathbf{x}'|} d^3x' = -\frac{1}{4\pi}\nabla \times \int \frac{\omega}{|\mathbf{x}-\mathbf{x}'|} d^3x'. \tag{30}$$

We now assume that the vorticity distribution is a *vortex filament*. This means that the vorticity distribution is confined to the near vicinity of a space curve. We parameterize the space curve via $\mathbf{R}(s)$, where s is the arc length. At every position on the space curve there is a local Frenet frame, namely an orthonormal frame where that is spanned by $\mathbf{n}(\mathbf{s})$ and $\mathbf{b}(\mathbf{s})$, with $\mathbf{n}, \mathbf{b}$ the normal and binormal to the curve. The vorticity distribution is then given by

$$\omega = \mathbf{t}(s)\omega_0(n, b), \tag{31}$$

where n, b are the coordinates in the local Frenet frame, at a given arc length s.

Taking into account the Jacobian of the transformation from cartesian coordinates to the curvilinear coordinates (s, n, b), $\frac{D(x,y,z)}{D(s,n,b)} = (1 - n/r_c)$, we can then rewrite Eqn. (30) as

$$\mathbf{v} = -\frac{1}{4\pi}\nabla \times \int \frac{\omega_0(n, b)\mathbf{t}(s)}{|\mathbf{x} - \mathbf{R}'(s, n, b)|}(1 - n/r_c)\text{ds dn db}, \tag{32}$$

where $\mathbf{R}'(s,n,b) = \mathbf{R}(s) + n\ \mathbf{n}(\mathbf{s}) + b\ \mathbf{b}(s) = \mathbf{R}(s) + \mathbf{x}'$, with $\mathbf{x}' = n\ \mathbf{n}(s) + b\ \mathbf{b}(s)$. Note that our coordinate system is such that $n = b = 0$ corresponds to the center of the filament. To proceed, we carry out a multipole distribution of the kernel of the integral. Namely, we write

$$\frac{1}{|\mathbf{x}-\mathbf{R}'|} = \frac{1}{|\mathbf{x}-\mathbf{R}(s)|} + \frac{(\mathbf{x}-\mathbf{R}(s))\cdot\mathbf{x}'}{|\mathbf{x}-\mathbf{R}(s)|^3} + \frac{\frac{3}{2}((\mathbf{x}-\mathbf{R}(s))\cdot\mathbf{x}')^2 - \frac{1}{2}|\mathbf{x}'|^2|\mathbf{x}-\mathbf{R}(s)|^2}{|\mathbf{x}-\mathbf{R}(s)|^5} + \cdots . \tag{33}$$

Using this in Eqn. (32), we find the leading order term

$$\mathbf{v} = -\frac{\Gamma}{4\pi}\nabla \times \int \mathrm{ds}\frac{\mathbf{t}(s)}{|\mathbf{x}-\mathbf{R}(s)|}, \tag{34}$$

where $\Gamma = \int \mathrm{dn\ db}\ \omega_0(n,b)$ is the circulation in the filament. This is the usual Biot Savart law. The extra terms in Eq. (33) give corrections to the Biot Savart law.

The first correction, induced by the curvature of the filament, results from the dipolar term and from the Jacobian, is expressed as: (our coordinate system is such that $n = b = 0$ corresponds to the center of the filament)

$$-\frac{1}{4\pi r_c}\nabla \times \int \mathrm{ds\ dn\ db}\ n^2\ \omega_0(n,b)\frac{(\mathbf{x}-\mathbf{R}(s))\cdot\mathbf{n}(s)}{|\mathbf{x}-\mathbf{R}(s)|^3} \tag{35}$$

The next nontrivial correction occurs at the next order, which gives

$$-\frac{1}{4\pi}\nabla \times \int \mathrm{ds\ dn\ db}\ \omega_0(n,b)\frac{\frac{3}{2}((\mathbf{x}-\mathbf{R}(s))\cdot\mathbf{x}')^2 - \frac{1}{2}|\mathbf{x}'|^2|\mathbf{x}-\mathbf{R}(s)|^2}{|\mathbf{x}-\mathbf{R}(s)|^5}, \tag{36}$$

We define two length scales, A and B, characterizing the shape of the filament:

$$A^2 = \frac{\int\ \mathrm{dn\ db}\ n^2\ \omega_0(n,b)}{\int\ \mathrm{dn\ db}\ \omega_0(n,b)} \quad \text{and} \quad B^2 = \frac{\int\ \mathrm{dn\ db}\ b^2\ \omega_0(n,b)}{\int\ \mathrm{dn\ db}\ \omega_0(n,b)}. \tag{37}$$

The two correction terms in Eq. (35) and Eq. (36) then reduce to:

$$-\frac{1}{4\pi r_c}\nabla \times \int \mathrm{ds}\ A^2\ \omega_0(n,b)\frac{(\mathbf{x}-\mathbf{R}(s))\cdot\mathbf{n}(s)}{|\mathbf{x}-\mathbf{R}(s)|^3} \tag{38}$$

and:

$$-\frac{\Gamma}{4\pi}\nabla \times \int \mathrm{ds}\ \frac{((\mathbf{x}-\mathbf{R}(s))\cdot\mathbf{n}(s))^2A(s)^2 + (\mathbf{x}-\mathbf{R}(s))\cdot\mathbf{b}(s))^2B(s)^2}{|\mathbf{x}-\mathbf{R}(s)|^5}. \tag{39}$$

respectively.

We remark that these correction terms are smaller than the leading order term, Eq. (34), by $O(A/|\mathbf{x}-\mathbf{R}|, B/|\mathbf{x}-\mathbf{R}|, A^2/(r_c|\mathbf{x}-\mathbf{R}|)$. Thus as long as the characteristic scales of the filament core are small relative to the interfilament distance and radius of curvature, the correction is negligible. However, if the cross section of the core is stretched sufficiently, so that it is of order the interfilament distance – then the Biot-Savart similarity solution breaks down.

APPENDIX B: OTHER POTENTIAL INSTABILITY MECHANISMS OF TWO CLOSELY INTERACTING VORTEX SHEETS

The iterative mechanism leading to a singularity presented in the manuscript rests on the postulated destabilization of vortex sheets due to the well-known Rayleigh mechanism [27]. It remains to demonstrate whether this assumption is actually valid in the particular flow configurations studied here. One of the potential difficulties comes from the short separation between the flattened vortex sheets. Whereas the Rayleigh mechanism is certainly valid for isolated (non-interacting) vortex sheets, possible complications are to be expected when two sheets are very close to each other, as it was found to be the case in the simulations summarized in Fig. 2a,b. In fact, the Rayleigh mechanism of instability was found to operate neither in our own simulations, nor, in fact, in any of the previously published simulations [9–13]. While this statement does not guarantee that the Rayleigh instability could not be the relevant instability mechanism in some flow configurations, we discuss here an alternative mechanism leading to a strong concentration of vorticity in strongly interacting vortex sheets, relevant to the configurations already studied.

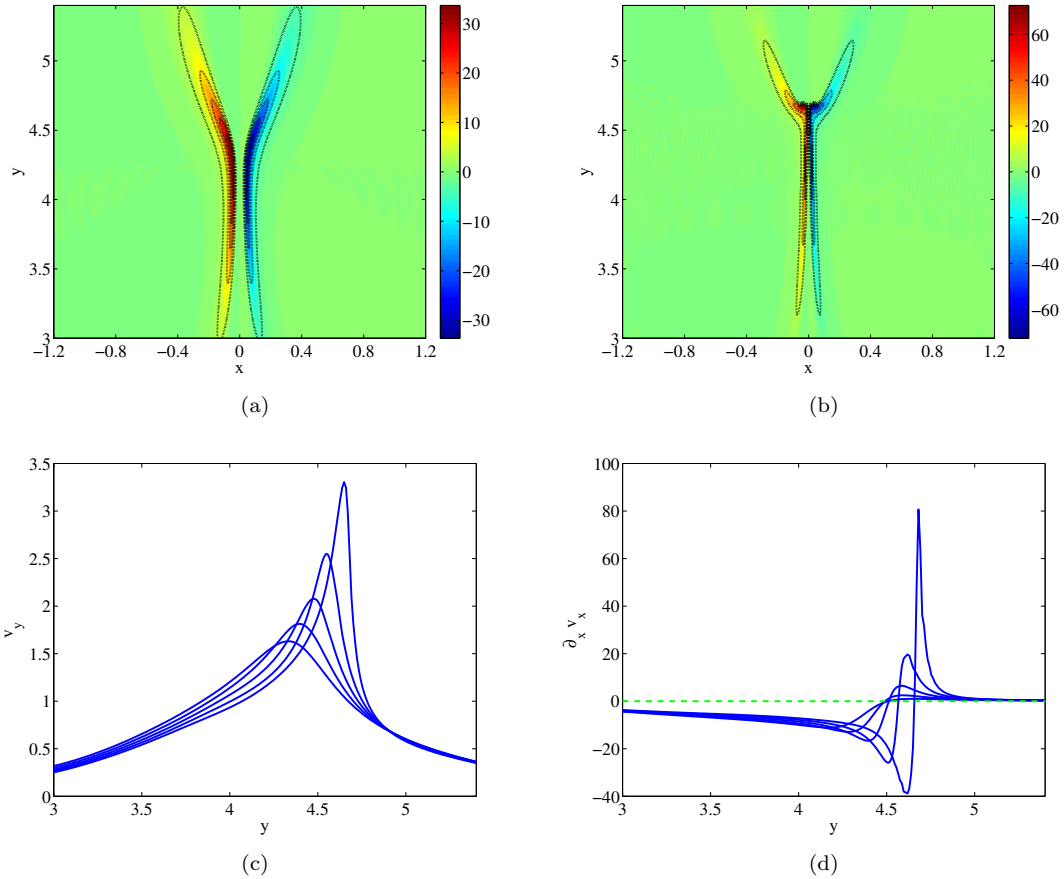

FIG. 4. Spontaneous formation of a kink from two curved vortex structures, initialized as two anti-parallel sheets in the region of close interaction. The initial condition of this simulation consisted in making the core structure flat in the plane $z = 0$, by introducing two different length scales for the vorticity distribution. As the vortices evolve, they developing two regions branching off perpendicular to the symmetry axis $y = 0$, as clearly seen in panel (b). This is a consequence of the strong increase of the velocity component in the y direction, see (c). As a result, the gradient $\partial_y v_y$ becomes very negative ahead of the region with maximum velocity (see d). Because of incrompessibility, $\partial_x v_x$ becomes positive, creating a structure with a sharp angle. The profiles shown in (c) and (d) are equally spaced in time, the first one corresponding the the solution shown in (a), and the last one to the solution shown in (b).

i

We illustrate our mechanism with the simulation of two vortex tubes, with a vorticity distribution centered around two filaments given by Eq. 3 of the main text, with parameters $A_T = 3.2$, $R_0 = 0.9$ and $\delta^2 = 1.24$. In these runs, we chose a non-circular distribution of vorticity in planes $z = \text{const}$. Specifically, we compressed the vorticity distribution by a factor $f = (1/0.12)^{1/2} \approx 2.9$ in the x-direction, and to stretch it by the same factor in the y-direction close to the plane of symmetry $z = 0$. The compression factor f relaxes towards 1 smoothly away from the symmetry plane. This configuration is convenient to study the interaction of vortex sheets, which is very relevant to the study of the present work.

Elementary fluid mechanics considerations show that the flow in between two sheets of anti-parallel vorticity correspond to a jet. In the configurations shown in Fig. 4(a,b), the velocity is positive in the y-direction. The y-component of the velocity decays away from the region where vorticity is concentrated.

In the flow we are considering, the sheets are pushed towards each other by a local compression close to the plane of symmetry $x = 0$. As the sheets are coming closer together, the velocity in the jet in between the two vortex sheets strongly increases, as an elementary consequence of the flow incompressibility. In particular, this leads to a steepening of the velocity profile $v_y(x = 0, y, z = 0)$ on the plane of symmetry, as shown in Fig. 4(c). The pinching of the vortices near the leading edge implies, as a consequence, a strong increase of the y-component of the velocity, followed by a very sharp decay. In particular, this leads to strongly negative values of the partial derivative $\partial_y v_y$. As the front steepens, we find that the overall stretching along the z-direction, $\partial_z v_z$, remains approximately constant, as it was

the case in the configuration of two initially parallel vortex tubes [10]. As a consequence of the incompressibility condition, $\partial_x v_x = -(\partial_y v_y + \partial_z v_z)$, the value of $\partial_x v_x$ ultimately becomes positive in the region ahead of the two vortices, as shown by Fig. 4(d). This flow configuration pushes the vortex sheets in a direction orthogonal to the axis of symmetry, thus generating a structure with a sharp angle, clearly seen in Fig. 4(b), and reported in many other similar simulations [10, 11].

This argument indicates that the formation of the sharp structures observed many times is an intrinsic feature of the interaction of vortex structures driven by the interaction of two vortex filaments in three-dimensional flows. We briefly mention here that we explicitly checked that the observation of a strong steepening of the y-component of the velocity component was also seen in other configurations, such as those shown in Fig. 2(b) of the main text. The only qualitative difference between the case of initially parallel vortex sheets (Fig. 4) and the case of intially parallel vortex tubes comes from the location where the cuspy point of the vorticity distribution develops. It is always located at the very front end in the latter case, whereas it develops in some intermediate position if the former.

Although the mechanism discussed here is fundamentally different from the roll-up which happens spontaneously for an isolated vortex sheet, it leads to the same physical consequences, namely, to a concentration of vorticity at some well defined regions of space, thus breaking the sheet structures to generate a tube-like structure. In addition, the extent of the region of the sheet involved in the formation of the rolling-up region, and thus in the formation of new filaments, is ≈ 10 times the width of the sheets. This suggests that the constant C, introduced in (16), is comparable to the one based on the instability calculation, see Section V, used throughout this work. All our numerical simulations, in agreement with previous numerical results, show that the vorticity is consistently highest in the region developing a sharp angle. Taken together, these observations indicate that the vorticity distribution within the strongly interacting sheets will bulge, thus leading to a very concentrated vortex structure, i.e., plausibly giving rise to a vortex tube.

APPENDIX C: ESTIMATING PREFACTORS FROM NUMERICAL SIMULATIONS OF THE EULER EQUATIONS

Here, we examine the deformation of the filament core, as shown in Fig. 2a of the main text, to determine the time evolution of a and b. We find, see Fig. 5, that the growth of a is much slower than the decrease of b, consistent with previous numerical studies of interacting vortex tubes [10, 11, 13]. The data is qualitatively very well fit by power laws, although over a limited range. Specifically, we find that $b \propto (t^* - t)^\alpha$, with $\alpha \approx 1$, and a grows with a significantly slower power law: $a \propto (t^* - t)^{-\beta}$, with $\beta \approx 1/3$. The limited resolution in the direct numerical simulations carried out here prevents a very accurate determination of the exponents α and β. Nonetheless, these values are fully consistent with the analytic results from the Biot-Savart analysis. Interestingly, the value of α suggested by the numerics satisfies $\alpha > 1/2$, which in turn suggests the existence of a negative fixed point of the iteration [22] of the main text, suggesting the formation of a singular solution.

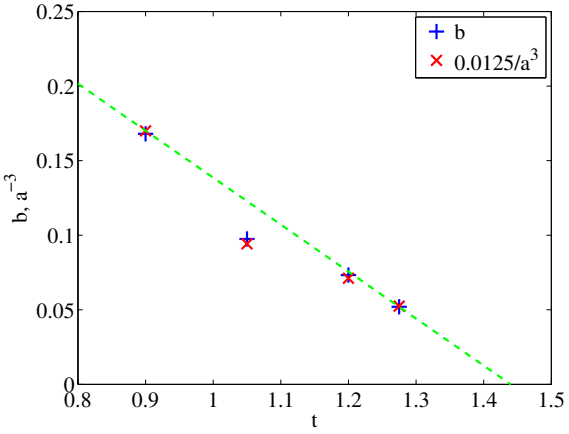

FIG. 5. Evolution of the sizes a, b of the core size in the plane $z = 0$, as a function of time. While b decays plausibly like $\propto (t^* - t)$, the size of the sheets increases slowly, like $b \propto (t^* - t)^{1/3}$, at least over a range of scales. The initial condition of this calculation was chosen to be $R_0 = 0.9$, $A_T = 3.5$ and $\delta^2 = 0.625$.

[1] G. I. Taylor and A. E. Green, "Mechanism of the production of small eddies from large ones," Proc. Roy. Soc. A **158**, 499–521 (1937).
[2] C. L. Fefferman, "The millennium prize problems," (Clay Mathematics Institute, Cambridge, MA, 2006) pp. 57–67.
[3] J. Leray, "Sur le mouvement d'un fluide visqueux emplissant l'espace," Acta Mathematica **63**, 193–248 (1934).
[4] L. Caffarelli, R. Kohn, and L. Nirenberg, "Partial regularity of suitable weak solutions of the navier-stokes equations," Comm. Pure and Appl. Math. **35**, 771–831 (1982).
[5] J. T. Beale, T. Kato, and A. Majda, "Remarks on the breakdown of smooth solutions for the 3d euler equations," Comm. Math. Physics **94**, 61–66 (1984).
[6] P. Constantin, "Singular, weak and absent: solutions of the euler equations," Physica D **237**, 1926–1931 (2008).
[7] D. Chae, "Non-existence of self-similar singularities for the 3d incompressible euler equations," Commun. Math. Phys. **270**, 203–215 (2007).
[8] M. E. Brachet, D. I. Meiron, S. A. Orszag, B. G. Nickel, R. H. Morf, and U. Frisch, "Small-scale structures on the taylor-green vortex," J. Fluid Mech. **130**, 411–452 (1983).
[9] A. Pumir and R. M. Kerr, "Numerical simulation of interacting vortex tubes," Phys Rev Lett **58**, 1636–1639 (1987).
[10] A. Pumir and E. D. Siggia, "Collapsing solutions of the 3d euler equations," Phys Fluids **A 2**, 220–241 (1990).
[11] R. M. Kerr, "Evidence for a singularity of the three-dimensional, incompressible euler equations," Phys Fluids **A 5**, 191–204 (1993).
[12] R. Pelz, "Locally self-similar, finte-time collapse in a high sy of strained vortex layers and vortex tube formation in homogeneous turbulence," Phys. Rev. Lett. **55**, 1617–1626 (1997).
[13] Y. T. Hou and R. Li, "Absence of singular stretching of interacting vortex filaments," J. Nonlinear Sci. **16**, 639–664 (2006).
[14] G. Luo and T. Y. Hou, "Potentially singular solutions of the 3d axisymmetric euler equations," Proc. Natl. Acad. Sci. USA **111**, 12968–12973 (2014).
[15] T. Tao, "Finite time blowup for an averaged three dimensional navier-stokes equation," arXiv.1402.0290 (2014).
[16] E. D. Siggia, "Origin of intermittency in fully developed turbulence," Phys. Rev. A **15**, 1730–1750 (1977).
[17] E. D. Siggia, "Collapse and amplification of a vortex filament," Phys Fluids **28**, 794–805 (1985).
[18] A. Pumir and E. D. Siggia, "Vortex dynamics and the existence of solutions to the navier-stokes equations," Phys Fluids **30**, 1606–1626 (1987).
[19] S. Childress, "Growth of anti-parallel vorticity in euler flows," Physica D: Nonlinear Phenomena **237**, 1921–1925 (2008).
[20] S. Hormoz and M. P Brenner, "Absence of singular stretching of interacting vortex filaments," J. Fluid Mech. **707**, 191–204 (2012).
[21] A. Pumir, "A numerical study of pressure fluctuations in three-dimensional, incompressible, homogeneous, isotropic turbulence," Phys. Fluids **6**, 2071–2083 (1994).
[22] T. S. Lundgren and W. T. Ashurst, "Area-varying waves on curved vortex tubes with application to vortex breakdown," J. Fluid Mech. **200**, 283–307 (1989).
[23] R. Klein, A. Majda, and K. Damodaran, "Simplified equations for the interaction of nearly parallel vortex filaments," Journal of Fluid Mechanics Digital Archive , 790 (2006).
[24] S. Kida, "Motion of an elliptic vortex in a uniform shear flow," Journal of the Physical Society of Japan **50**, 3517–3520 (1981).
[25] J. C. Neu, "The dynamics of stretched vortices," Journal of Fluid Mechanics **143**, 253–276 (1984).
[26] J. C. Neu, "The dynamics of a columnar vortex in an imposed strain," Physics of Fluids (1958-1988) **27**, 2397–2402 (1984).
[27] Lord Rayleigh, "On the stability, or instability of certain fluid motion," Proc. Lond. Math. Soc. **11**, 57–72 (1880).
[28] T. Passot, H. Politano, P. L. Sulem, J. R. Angilella, and M. Meneguzzi, "Instability of strained vortex layers and vortex tube formation in homogeneous turbulence," J. Fluid Mech. **282**, 313–338 (1995).
[29] ATAM De Waele and RGKM Aarts, "Route to vortex reconnection," Phys. Rev. Lett. **72**, 482 (1994).
[30] L. Boué, D. Khomenko, V. S. L'vov, and I. Procaccia, "Analytic solution of the approach of quantum vortices towards reconnection," Phys. Rev. Lett. **111**, 145302 (2013).
[31] A. Pumir, B. I. Shraiman, and E. D. Siggia, "Vortex morphology and kelvin's theorem," Phys Rev A **45**, R5351–5354 (1992).
[32] Y. Pomeau and D. Sciamarella, "An unfinished tale of nonlinear pdes: Do solutions of 3d incompressible euler equations blow-up in finite time ?" Physica D Fluids **205**, 215–221 (2005).
[33] P. Cvitanović, "Recurrent flows: the clockwork behind turbulence," J. Fluid Mech. **726**, 1–4 (2013).
[34] W. T. Ashurst and D. I. Meiron, "Numerical study of vortex reconnection," Phys. Rev. Lett. **58**, 1632–1635 (1987).
[35] Y. Oshima, T. Kambe, and S. Asaka, "Interaction of two vortex rings moving along a common axis of symmetry," J. Phys. Soc. Japan **38**, 1159–1166 (1975).
[36] T. Fohl and J. S. Turner, "Colliding vortex rings," Phys. Fluids **18**, 433–436 (1975).
[37] T. T. Lim and T. B. Nickels, "Instability and reconnection in the head-on collision of vortex rings," Nature **357**, 225–227 (1992).
[38] D. Kleckner and W. T. M. Irvine, "Creation and dynamics of knotted vortices," Nature Phys. **9**, 253–258 (2013).
[39] Y. Kimura and H. K. Moffatt, "Reconnection of skewed vortices," J. Fluid Mech. **751**, 329–345 (2014).
[40] P. G. Saffman, "A model of vortex reconnection," J. Fluid Mech. **212**, 395–404 (1990).

[41] M. J. Shelley, D. I. Meiron, and S. A. Orszag, "Dynamical aspects of vortex reconnection of perturbed anti-parallel vortex tubes," J. Fluid Mech. **246**, 613–652 (1993).
[42] A. Pumir and E. D. Siggia, "Finite-time singularities in the axisymmetric three-dimension euler equations," Phys. Rev. Lett. **68**, 1511 (1992).